Supporting information

1. Experimental Section

1.1. Materials

Stannic Chloride ($SnCl_4$, 99%), Polyvinylpyrrolidone (PVP, K-30, molecular weight ~40000), Manganese Chloride tetrahydrate ($MnCl_2.\ 4H_2O$, 97%), and Nickel Chloride hexahydrate ($NiCl_2.6H_2O$, 97%) were purchased from SRL Chemicals. HPCL-grade ethanol (97%) was purchased from HiMedia. Sodium hydroxide and potassium hydroxide (85%) were purchased from Alfa Aesar. Fluorine-doped tin oxide (FTO) of surface resistivity 7 Ω was purchased from Sigma Aldrich. Nickel foam was purchased from DTech Solution, India. All the reagents were used without any further purification.

1.2. Material Synthesis

1.2.1. Synthesis of $Na_2Sn(OH)_6$

0.36 g PVP was dissolved in 20 mL of ethanol/water (4: 1 in volume) mixed solvent solution, after which 1 mL of $SnCl_4$ was added dropwise under continuous stirring.[1] After vigorous stirring for 10 min, 10 mL of 12.5M NaOH solution was added to the above solution, with vigorous stirring being maintained for another 10 min. Next, the mixed solution was transferred to a 50 mL Teflon-lined hydrothermal autoclave and maintained at 180°C for 24 h to enable the following reaction to occur:

$$SnCl_4 + 6NaOH \longrightarrow Na_2Sn(OH)_6 \downarrow + 4NaCl \quad (1)$$

After being cooled to room temperature, the white precipitate formed in the autoclave was collected by vacuum filtration and washed with ethanol three times. Finally, the white powder was dried under a vacuum at room temperature for two days before further use.

1.2.2 Synthesis of manganese and manganese-nickel perovskite hydroxide

The Sn-based multicomponent oxides were prepared by a cation exchange reaction between the metal ion of interest and $Na_2Sn(OH)_6$ in an aqueous solution according to the following reactions:

$$M^{2+} + Na_2Sn(OH)_6 \longrightarrow MSn(OH)_6 \downarrow + 2Na^+ \quad (3)$$

In detail, under continuous stirring, 5 mL of 10 mM $Na_2Sn(OH)_6$ aqueous solution was added dropwise to a 5 mL aqueous solution containing 10 mM (Mn and Mn, Ni). The mixed solution

was stirred for a further 10 min and then centrifuged to isolate the precipitate, which was then washed with water and ethanol twice and dried under vacuum at room temperature.[1]

2. Materials' Characterization

X-ray diffraction patterns for materials were obtained from PANalytical powder XRD. Here, a position-sensitive detector, a curved germanium (111) primary monochromator, and a Cu-$K_{\alpha 1}$ radiation (λ = 1.5418 Å) was used. Scanning Electron Microscopy (SEM) was done to analyze the morphologies using an FEI NOVA NANOSEM 450 field emission scanning electron microscope under 10 kV electron gun energy. For mapping and elemental analysis, the SEM measurements were performed using 15 kV electron gun energy integrated with an energy dispersive X-ray (EDX) detector (Bruker Quantax XFlash® 6|60). Data handling and analyses were attained with the software package EDAX. The high-resolution TEM, HAADF-STEM, and the corresponding energy dispersive spectroscopy mapping analyses were performed on an FEI TECNAI G2 F30) transmission electron microscope (TEM 300kV) equipped with a LaB_6 source. The catalyst films were scratched off from the FTO substrate and transferred onto a carbon-coated copper grid for their investigation after catalysis. EDX analyses were achieved with an EDAX r-TEM SUTW (Si (Li) detector). GATAN MS794 P and GATAN US1000 CCD cameras were used to collect the images. The scanning TEM (STEM) experiments were conducted on a probe-corrected JEM-ARM300F2 "GrandARM2" (JEOL Ltd.) with cold-FEG emitter at 80 and 300 kV, equipped with 2 x 158mm² windowless SDD-EDX detectors with a solid angle of 2.2 sr. HAADF images correspond to detection angles of 54-220 mrad The X-ray photoelectron spectra (XPS) were acquired using an Omicron X-ray photoelectron spectrometer using Mg-K_{α} radiation at 1253.6 eV as the excitation source with an Al-K_{α} monochromatic radiation source (1486.7 eV) with a 90° takeoff angle (normal to analyzer). The vacuum pressure in the analyzing chamber was set at 2×10^{-9} Torr. The XPS spectra were collected for C 1s, O 1s, Ni 2p, Mn 2p, and Sn 2p levels with pass energy 20 eV and step 0.1 eV. The binding energies were calibrated relative to the C 1s peak energy position as 285.0 eV. Data analyses were carried out using Casa XPS (Casa Software Ltd.) and the Vision data processing program (Kratos Analytical Ltd.).

***In situ* Raman spectroscopy**

The *in situ* Raman spectra was recorded by exciting the samples using a 532 nm argon-laser. A confocal Raman spectrometer associated with a liquid nitrogen-cooled charge-coupled device camera as a detector (Renishaw). Water-immersion objective lens (40XW, Olympus, numerical

aperture: 0.8) covered with PFA film (0.05 mm thickness) was used in the home-built single chamber electrochemical cell. During measurement, a noncontact probe head with a working distance of 5 cm and a sample spot size of 1 mm was used. For every measurement, 5 s acquisition time was required. The Raman signal was recorded from the initial state of the prepared $MnNiSn(OH)_6$ film and its in situ OER and organic conversion reaction (0.0 to −0.8 V RHE) in 1.0 M KOH with a voltage interval of 0.1 V.

Electrophoretic deposition and electrochemical measurements

The investigated materials were electrophoretically deposited (EPD) on thoroughly cleaned nickel foam (NF) and fluorine doped tin oxide (FTO) by applying a potential difference of 10 V in a mixture of iodine and acetone.[2] The deposition was carried out on a 1 × 1 cm^2 area. For a typical deposition, 40 mg of the catalyst powder was suspended in 10 ml acetone, and 2 mg of iodine was then added. This solution is sonicated for 15 min and taken in a 10 ml glass beaker. Before EPD, the empty electrodes were weighted using an analytical balance. After each EPD, the increase in weight of the electrodes was monitored carefully. A catalyst loading of ~1.0 mg cm^{-2} and ~0.6 mg cm^{-2} on NF and FTO was achieved, respectively. The mass loading was reproducible within the margins of an experimental error (±0.1 mg).

The electrochemical testing was carried out in a standard three-electrode (working, counter, and reference) electrochemical cell in 1 M aqueous KOH with a potentiostat (VMP3,16 channel potentiostat from BioLogic Science Instruments) controlled by the EC-Lab v10.20 software package. The electrodes (NF/FTO) with deposited catalysts served as the working electrodes, Pt wire (0.5 mm diameter from DTech solution) as a counter, and Hg/HgO (D-Tech solution) as the reference electrode. All potentials presented in this work were transferred to the RHE scale by calibrating the reference electrodes versus an RHE electrode (+917 mV for 1 M KOH (pH 13.89)).[3]

The chronoamperometric measurements were performed in 1 M aqueous KOH at selected constant potentials with respect to RHE.

The voltammograms and chronoamperometry curves were recorded with an applied *iR* compensation of 90%. The uncompensated resistance was obtained from an impedance point measurement at 1.2 V_{RHE} and 100 kHz with an amplitude of 10 mV. Tafel plots were calculated by potentiostatic measurements between 1.4 and 1.6 V_{RHE}, employing stepwise potential changes by 20 mV. The current density at each potential was determined by taking the average of a 2-minute measurement. The Tafel slope was calculated according to the Tafel equation η

= $b\log j + a$, where η is overpotential (V), j is the current density (mA cm^{-2}), and b is the Tafel slope ($mVdec^{-1}$).

Bulk electrolysis of organic secondary alcohols

The voltammogram and bulk electrolysis investigations were performed in a three-electrode setup analogously to one of the OER studies. An NF with electrophoretically deposited $MnSn(OH)_6$ and $Mn(Ni)Sn(OH)_6$ was used as the anode, and a platinum wire as the cathode in a 50 mM alcohol solution containing 20 ml of 1 M KOH solution. For bulk electrolysis, CA experiments at 1.49 V_{RHE} were performed.

^{1}H NMR analysis of the organic compound

The oxidation reaction mixture was characterized by ^{1}H NMR spectroscopy in a Bruker AV400 instrument. The ^{1}H NMR sample was prepared by taking a 150 µL aliquot of the reaction mixture and 350 µL D_2O. Processing and plotting of the spectra were performed using MestReNova. A sharp peak at 4.7 ppm appeared for the H_2O from the aqueous reaction mixture and was used as a reference for the chemical shifts of the other proton signals.

Calculation of the faradaic efficiency, product yield for the oxidation of secondary alcohols (SAlc)

The Faradaic efficiency was calculated based on the ketone yield and charge passed during the bulk electrolysis. The product yield was calculated using ^{1}H NMR analysis. An internal standard, dimethylsulfoxide (DMSO), was used and the product protons were integrated. Depending on the structure and signal overlap, suitable sets of protons are used to calculate the yield. The required charge for full conversion ($Q_{100\%}$) was calculated using:

$$Q_{100\%} = m_{\mathrm{SAlc}} \times F \times n_e / M_{\mathrm{SAlc}}$$

Here, F is the Faraday constant (96485 C mol^{-1}), n_e is the number of electrons required for the oxidation process (2), m_{SAlc} is the weight of SAlc used for the reaction, and M_{SAlc} is the molecular weight of SAlc. This gives $Q_{100\%}$ = 192.97 C.

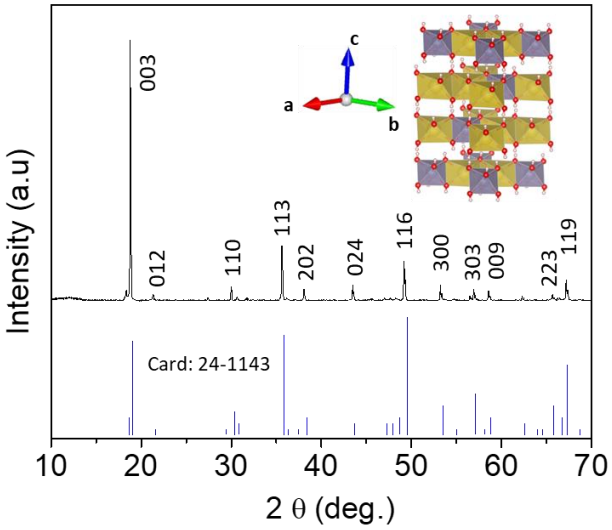

Figure S1. The XRD pattern of the as-prepared $Na_2Sn(OH)_6$ where all the reflections are indexed. The grey and yellow polyhedral represents the [Sn-O_6] and [Na-O_6] octahedra.

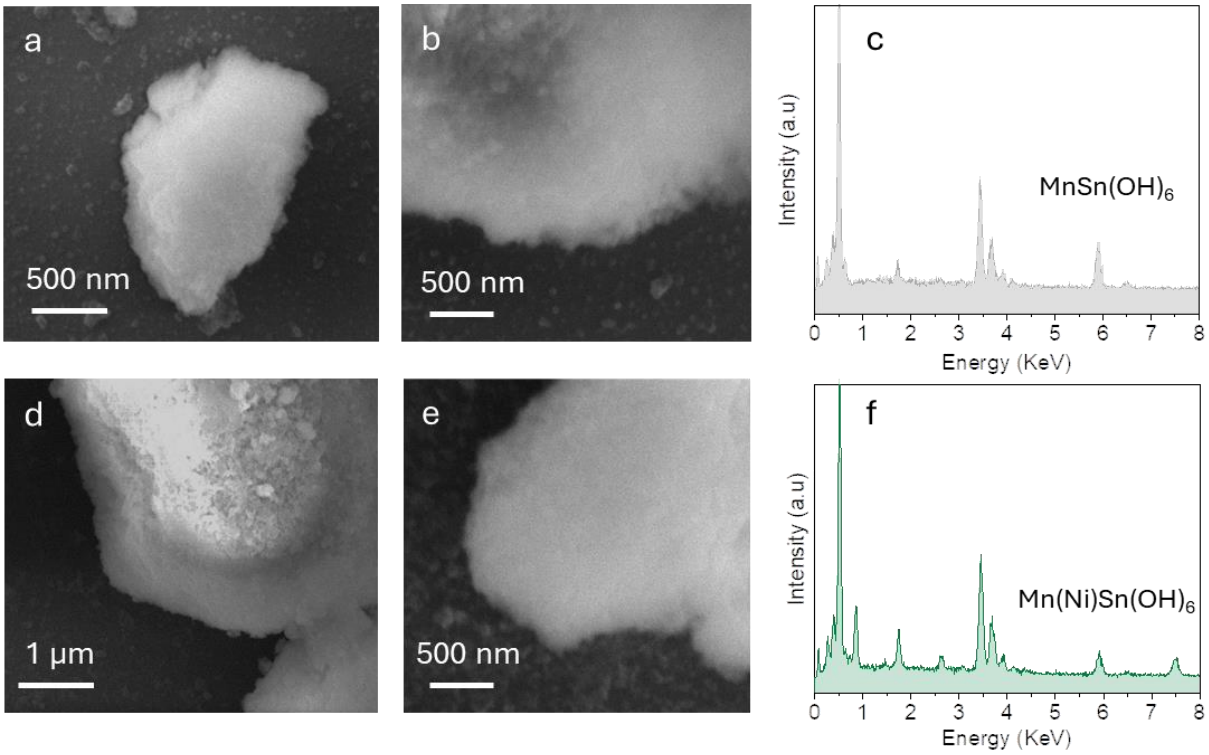

Figure S2. SEM image and corresponding EDX analysis of the (a-c) $MnSn(OH)_6$ and (d-f) $Mn(Ni)Sn(OH)_6$. The Mn to Sn ratio is 1:1.07 in the $MnSn(OH)_6$, whereas Mn, Ni, and Sn have a ratio of 1:0.94:1.1 in the $Mn(Ni)Sn(OH)_6$.

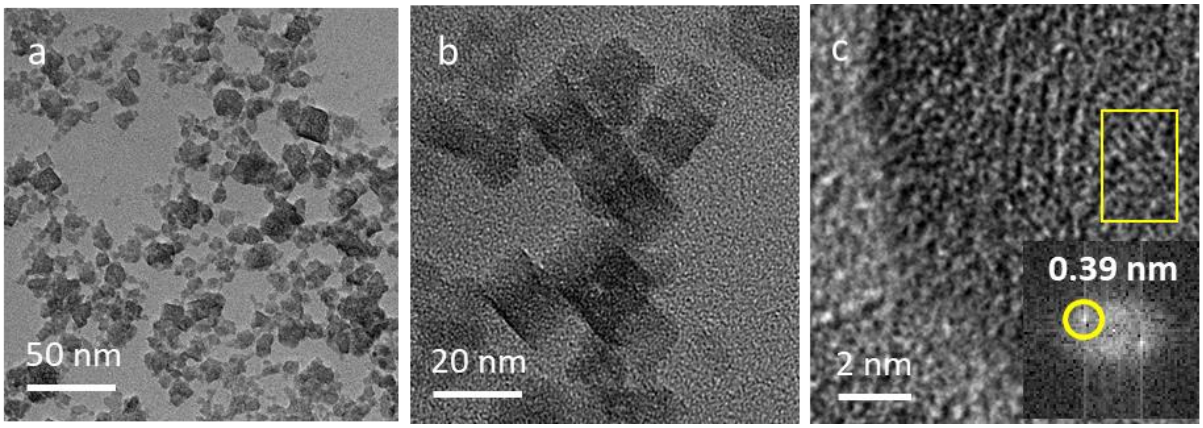

Figure S3. (a-c) TEM and HRTEM of as prepared $MnSn(OH)_6$ (TEM of $Mn(Ni)Sn(OH)_6$ is in Figure 1, main text). TEM shows an irregular cubic shaped morphology with sharp edge. Inset of fig. c shows the FFT transformed lattice planes, which attributes to (200) planes of the $MnSn(OH)_6$.

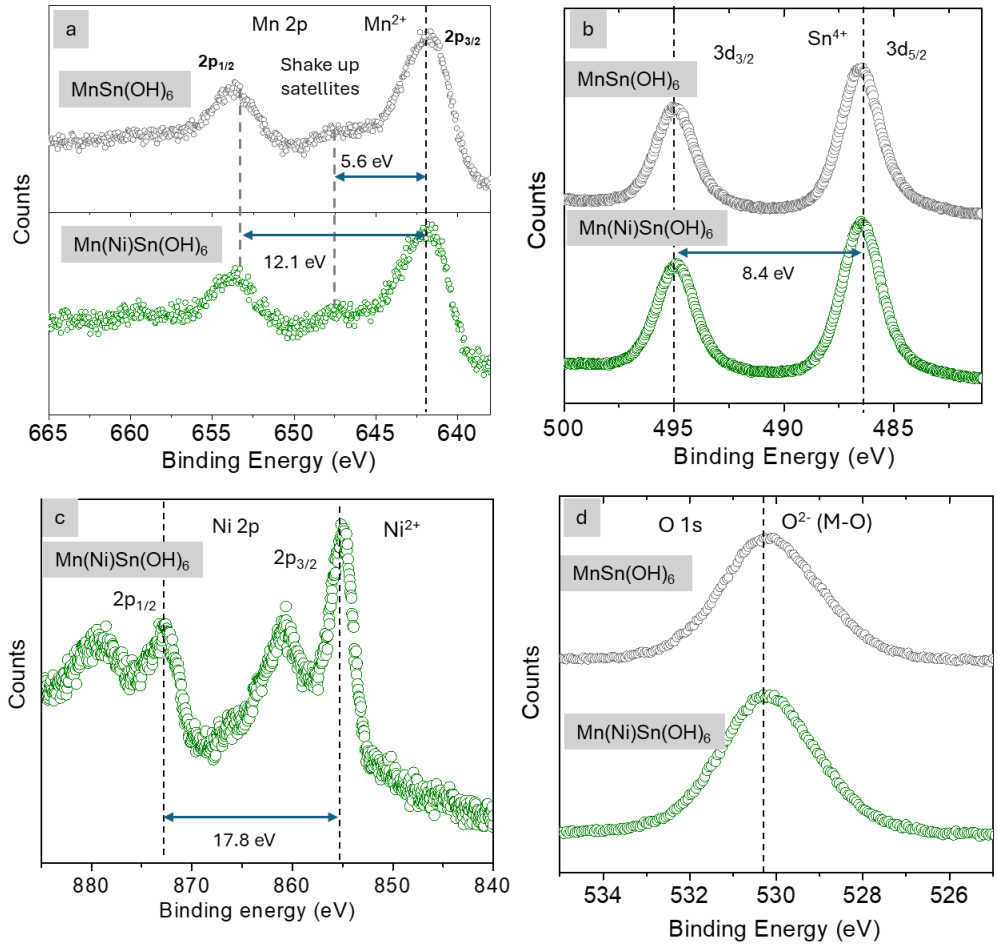

Figure S4. High resolution Mn 2p, Ni 2p, Sn 3d and O 1s XPS profile of the as-prepared $MnSn(OH)_6$ and $Mn(Ni)Sn(OH)_6$ confirmed the oxidation of state of Mn^{II+}, Ni^{II+}, Sn^{IV+} and O^{II-}.[4,5]

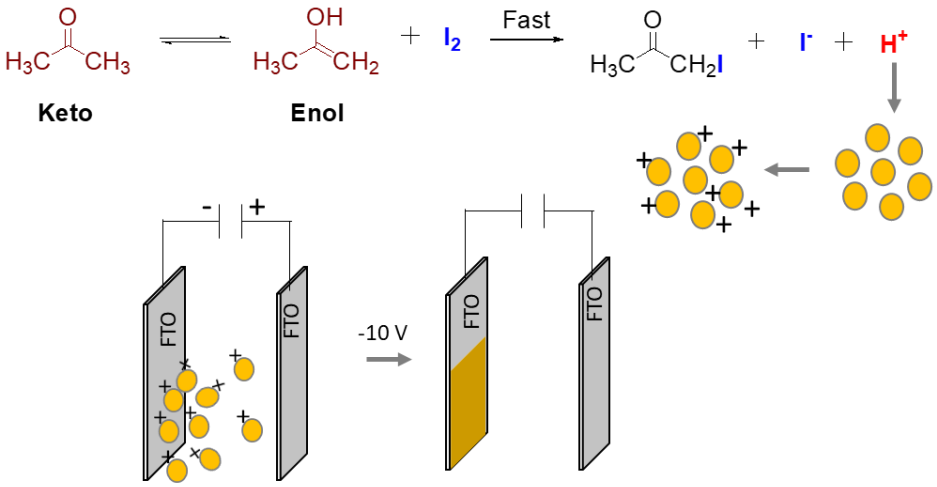

Figure S5. Schematic representation for the electrophoretic deposition of as-prepared (pre)catalyst nanostructure (shown as yellow ball) on the conductive substrate (as a representative FTO glass plate is shown here).

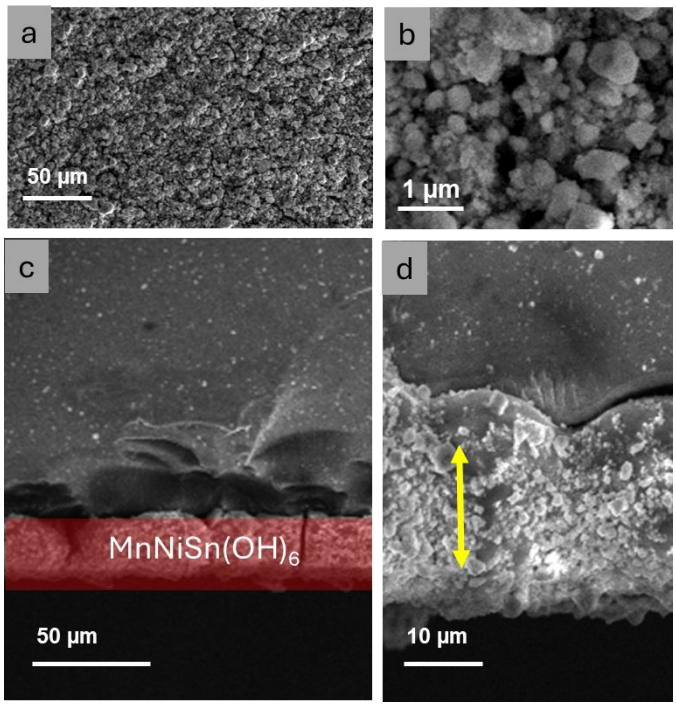

Figure S6. The (a,b) top view and (c,d) side view SEM image of electrophoretically deposited $MnNiSn(OH)_6$ on the FTO substrate (as a representative (pre)catalyst)). The film is homogeneous and pinhole free. The average thickness of the film is estimated as 10 µm.

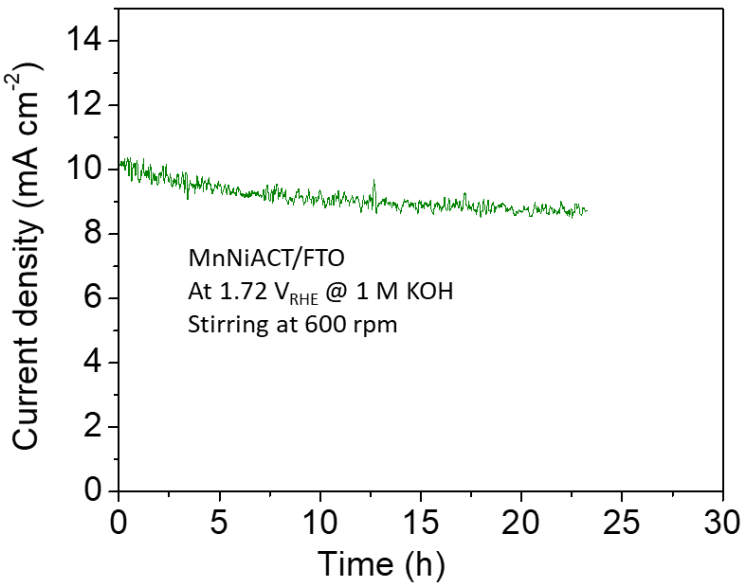

Figure S7. Chronoamperometry of the activated $Mn(Ni)Sn(OH)_6$ in 1 M KOH at 1.72 V_{RHE} indicates not a significant drop of current over more than 24 hours.

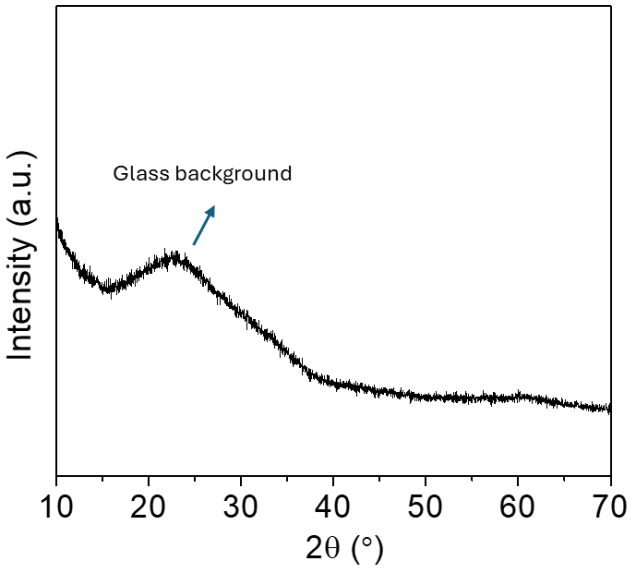

Figure S8. The powder XRD pattern of the $NiSn(OH)_6$, which appeared as XRD amorphous material. The synthesis method is similar as that of $MnNiSn(OH)_6$. This observation is similar to the previous report by Zhang et al.[1]

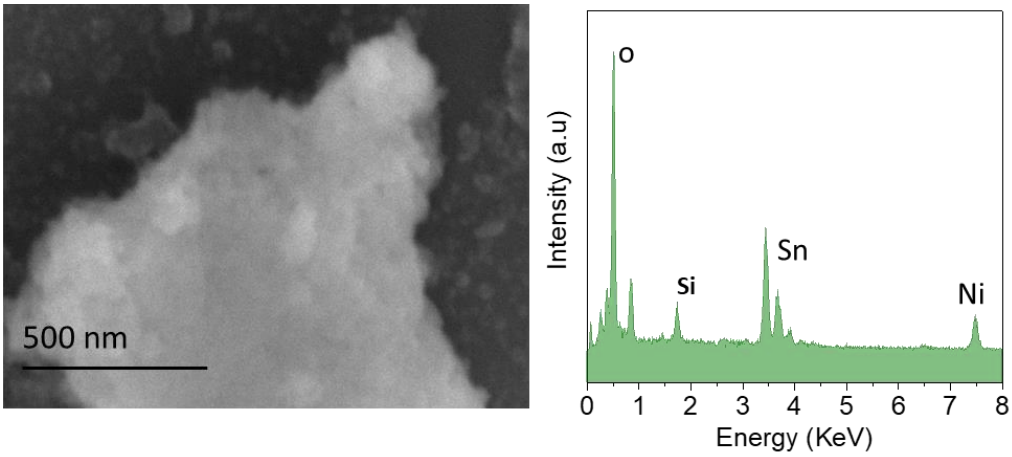

Figure S9. SEM image and corresponding EDX profile for the as-prepared $NiSn(OH)_6$. Si peak came from the substrate.

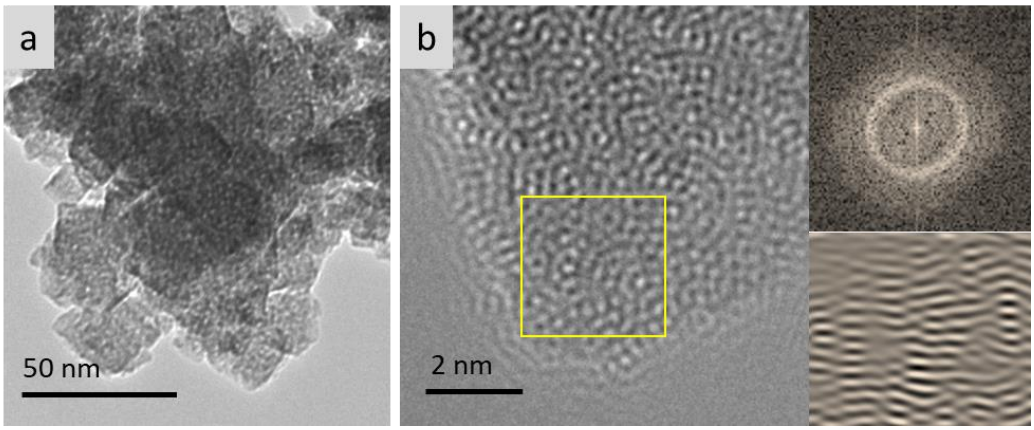

Figure S10. (a) low magnification and (b) high resolution TEM image of the $NiSn(OH)_6$. The FFT and inverse project are collected from the marked area shown in 'panel b'. The results show the structure is full of defects and X-ray amorphous.

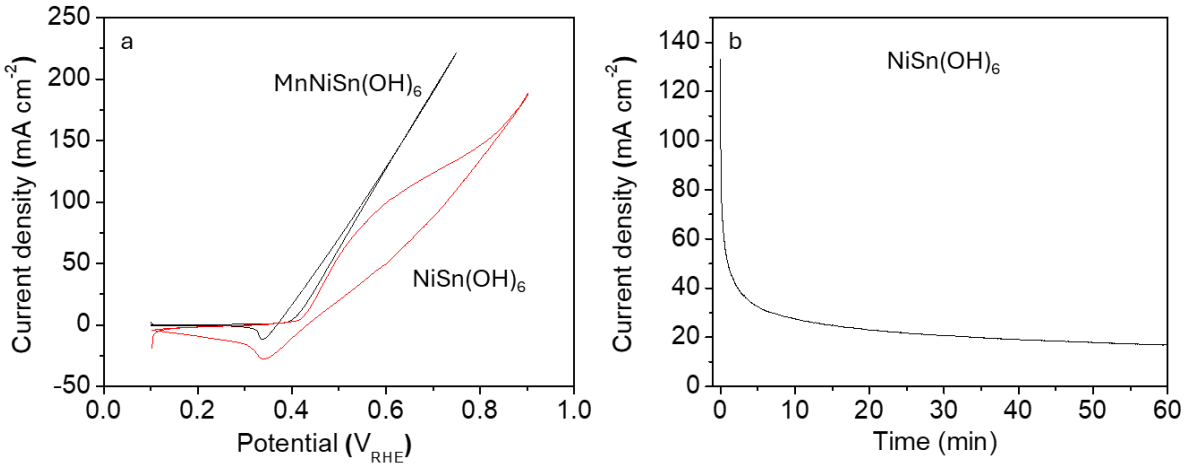

Figure S11. Electrochemical benzyl alcohol oxidation activity of $NiSn(OH)_6$.

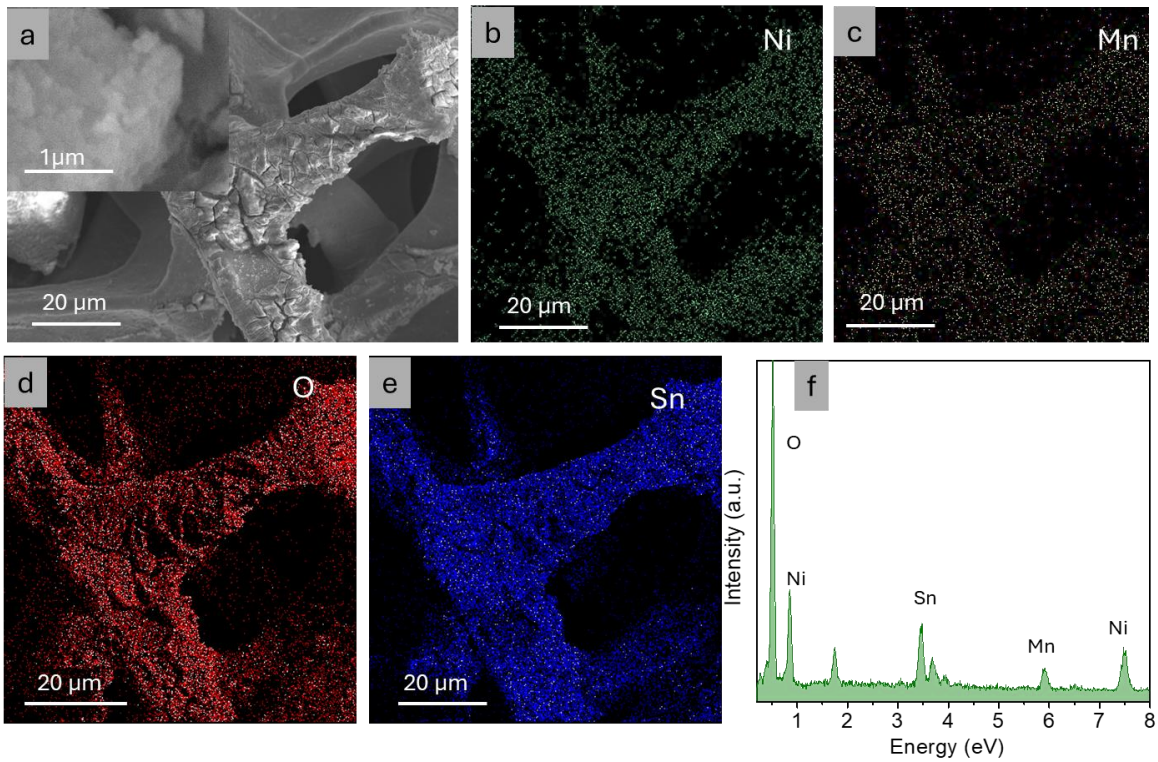

Figure S12. SEM image, corresponding elemental mapping, and EDX profile of the electrophoretically deposited $MnNiSn(OH)_6$ on the nickel foam substrate.

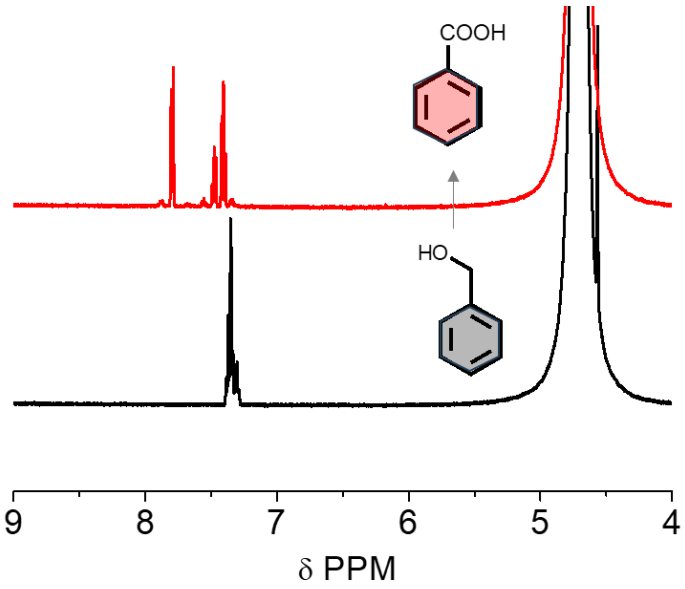

Figure S13. ^{1}H NMR spectra of before and after reaction (bulk electrochemical oxidation as shown in Figure 2e (main text) solution.

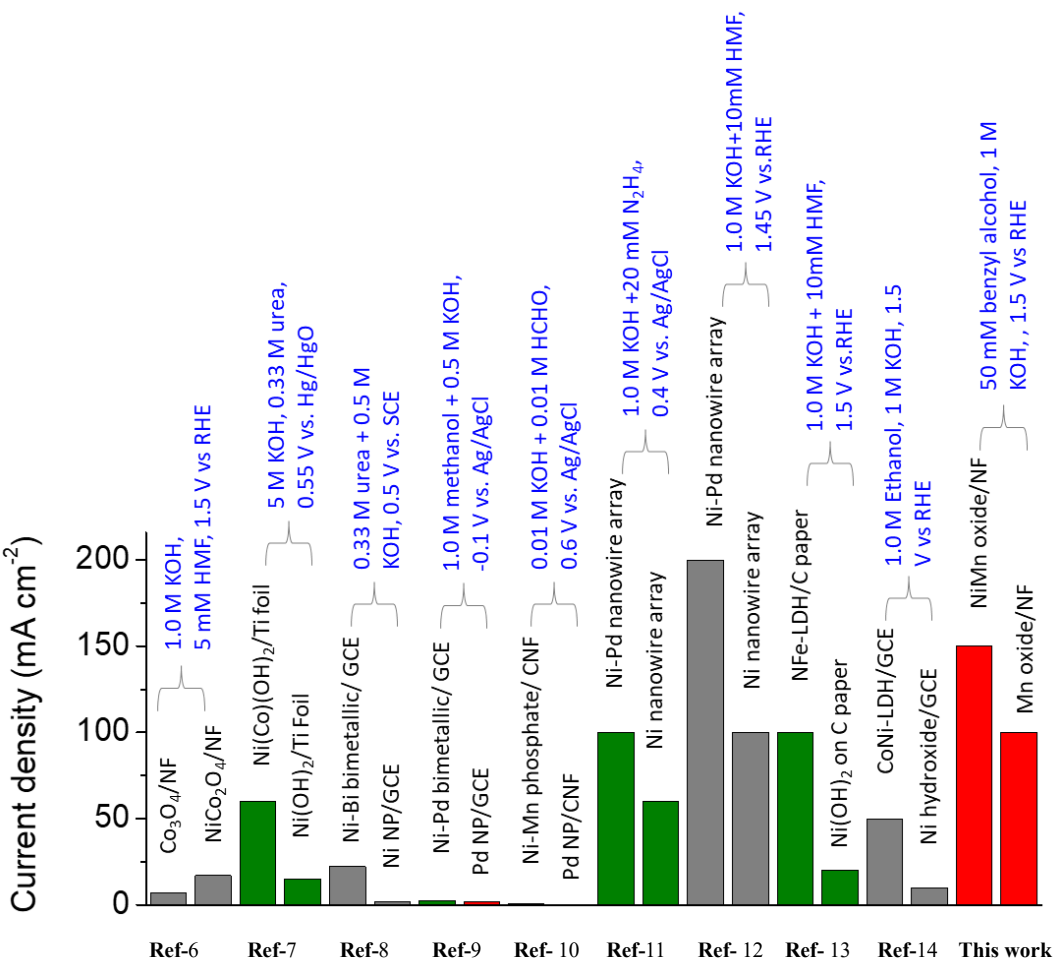

Figure S14. The activity bar-diagram for organic electro-oxidation using different heterobimetallic system reported previously.

Table S1. ICP analysis of the $Mn(Ni)Sn(OH)_6$ and $MnSn(OH)_6$ before and after benzyl alcohol oxidation.

$MnSn(OH)_6$	Before reaction	Mn (1.3 PPM)	Sn (1.25 PPM)	-	-
	After reaction	Mn (0.7 PPM)	Sn (0.17 PPM)	K (0.04 PPM)	-
$Mn(Ni)Sn(OH)_6$	Before reaction	Mn (1.62 PPM)	Ni (1.58 PPM)	Sn (1.6 PPM)	-
	After reaction	Mn (0.8 PPM)	Ni (0.76 PPM)	Sn (0.41 PPM)	K (0.01)

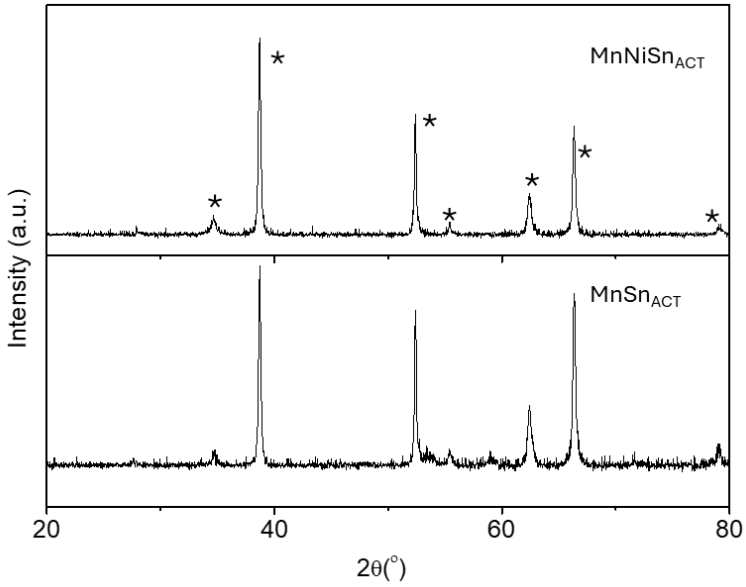

Figure S15. XRD of the catalysts after the benzyl alcohol oxidation reaction. The asterisk implies the FTO peak. The catalysts are x-ray amorphous.

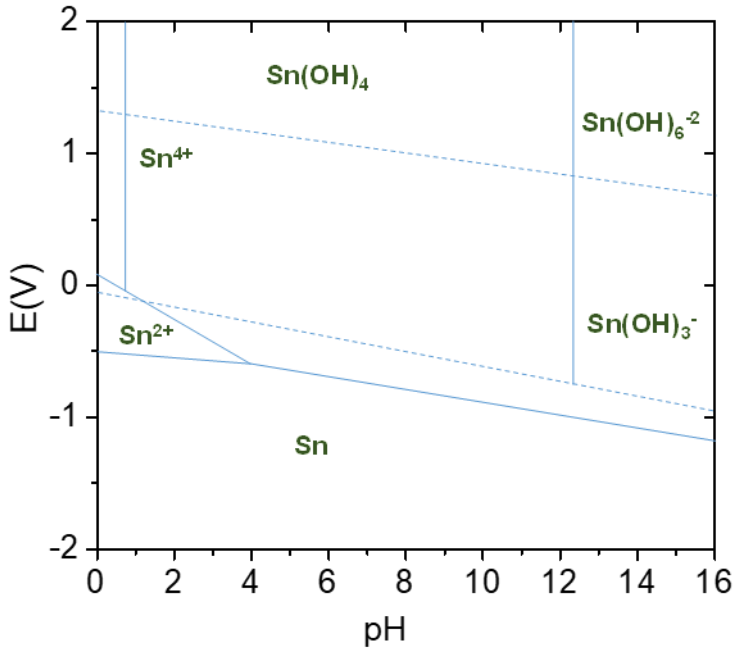

Figure S16. Pourbaix diagram of Sn-H_2O system. At pH 13.8 and the potential at which we carry our electrochemical measurements, Sn leaches as a partially soluble anionic species into the solution.[15]

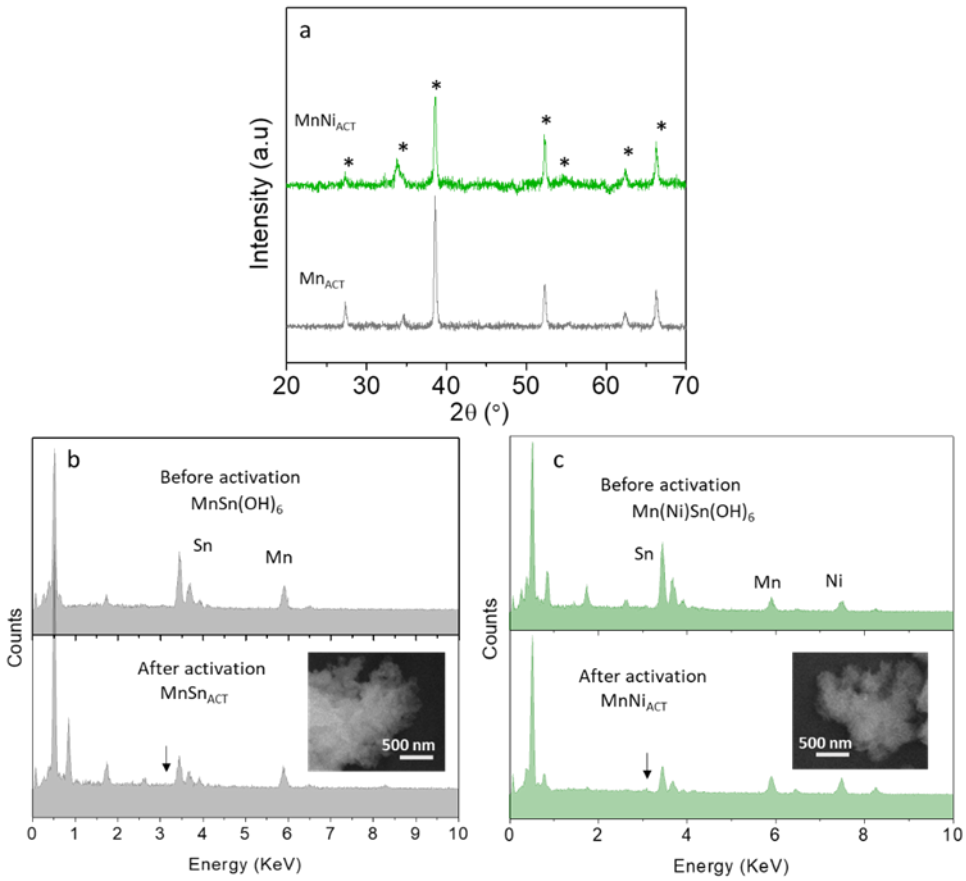

Figure S17. (a) The post-activation XRD pattern collected on the catalyst/FTO film (asterisk indicates the reflections from the FTO) (b,c) post-activation SEM-EDX of the catalyst suggests a significant Sn leaching, yet a similar Mn/Ni ratio as the (pre)catalyst.

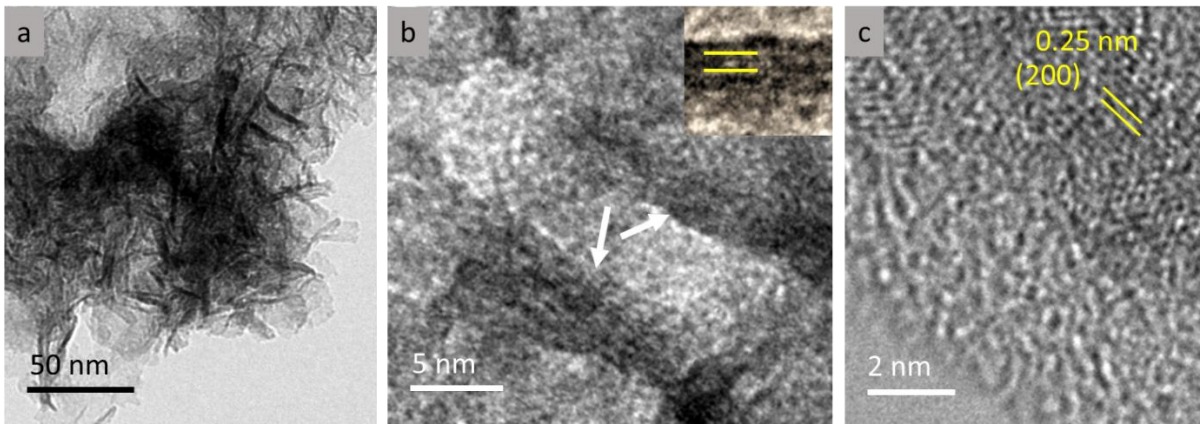

Figure S18. TEM morphology of $MnSn(OH)_6$ after benzyl alcohol oxidation. (a) low magnification image shows sheet-like structure, typical for layered (birnessite) manganese oxide (b) high magnification image of the nanostructure showing typical metal oxide layers (arrow indication) in set showing the 0.7 nm interlayer distance, (c) HRTEM showing the (200) plane of the birnessite top face.

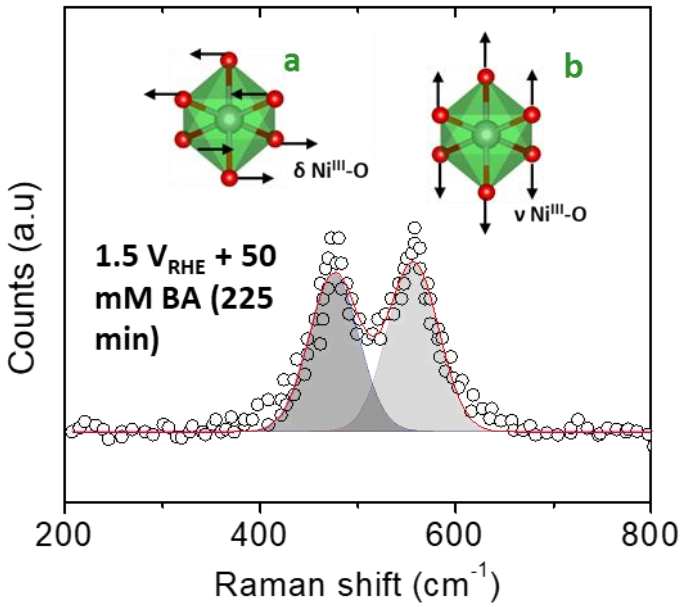

Figure S19. A gaussian fitting for the [Ni^{III}-O] vibration suggest a doublet (δ, and ν) in the Raman profile. The peak ratio for δ/ν suggests a mixture of γ-NiOOH and β-NiOOH.

References

1 X. Zhang, F. Li, Y. Zhang, A. M. Bond and J. Zhang, *J. Mater. Chem. A*, 2018, **6**, 7851–7858.

2 I. Mondal, J. N. Hausmann, G. Vijaykumar, S. Mebs, H. Dau, M. Driess and P. W. Menezes, *Adv. Energy Mater.*, 2022, **12**, 2200269.

3 J. N. Hausmann, B. Traynor, R. J. Myers, M. Driess and P. W. Menezes, *ACS Energy Lett.*, 2021, **6**, 3567–3571.

4 H. Li, Y. He, Q. Wang, S. Gu, L. Wang, J. Yu, G. Zhou and L. Xu, *Adv. Energy Mater.*, , DOI:10.1002/aenm.202302901.

5 G. Wang, X. Sun, F. Lu, Q. Yu, C. Liu and J. Lian, *J. Solid State Chem.*, 2012, **185**, 172–179.

6 M. J. Kang, H. Park, J. Jegal, S. Y. Hwang, Y. S. Kang and H. G. Cha, *Appl. Catal. B Environ.*, 2019, **242**, 85–91.

7 X. Yan, Q.-T. Hu, J. Liu, W.-D. Zhang and Z.-G. Gu, *Electrochim. Acta*, 2021, **368**, 137648.

8 A. V. Munde, B. B. Mulik, R. P. Dighole and B. R. Sathe, *ACS Appl. Energy Mater.*, 2021, **4**, 13172–13182.

9 L. Chen, H. Guo, T. Fujita, A. Hirata, W. Zhang, A. Inoue and M. Chen, *Adv. Funct. Mater.*, 2011, **21**, 4364–4370.

10 I. Elghamry, S. A. Al-Jendan, M. M. Saleh and M. E. Abdelsalam, *RSC Adv.*, 2022, **12**, 20656–20671.

11 M. Du, H. Sun, J. Li, X. Ye, F. Yue, J. Yang, Y. Liu and F. Guo, *ChemElectroChem*, 2019, **6**, 5581–5587.

12 G. Yang, Y. Jiao, H. Yan, Y. Xie, A. Wu, X. Dong, D. Guo, C. Tian and H. Fu, *Adv. Mater.*, DOI:10.1002/adma.202000455.

13 W.-J. Liu, L. Dang, Z. Xu, H.-Q. Yu, S. Jin and G. W. Huber, *ACS Catal.*, 2018, **8**, 5533–5541.

14 W. Wang, Y. Zhu, Q. Wen, Y. Wang, J. Xia, C. Li, M. Chen, Y. Liu, H. Li, H. Wu and

T. Zhai, *Adv. Mater.*, , DOI:10.1002/adma.201900528.

15 C. I. House and G. H. Kelsall, *Electrochim. Acta*, 1984, **29**, 1459–1464.